Grain Boundary Passivation of Multicrystalline Silicon Using Hydrogen Sulfide as a Sulfur Source

by

Arunodoy Saha

A Thesis Presented in Partial Fulfillment
of the Requirements for the Degree
Master of Science

Approved November 2014 by the
Graduate Supervisory Committee:

Meng Tao, Chair
Dragica Vasileska
Michael Goryll

ARIZONA STATE UNIVERSITY

December 2014

ABSTRACT

Hydrogen sulfide (H_2S) has been identified as a potential ingredient for grain boundary passivation of multicrystalline silicon. Sulfur is already established as a good surface passivation material for crystalline silicon (c-Si). Sulfur can be used both from solution and hydrogen sulfide gas. For multicrystalline silicon (mc-Si) solar cells, increasing efficiency is a major challenge because passivation of mc-Si wafers is more difficult due to its randomly orientated crystal grains and the principal source of recombination is contributed by the defects in the bulk of the wafer and surface.

In this work, a new technique for grain boundary passivation for multicrystalline silicon using hydrogen sulfide has been developed which is accompanied by a compatible Aluminum oxide (Al_2O_3) surface passivation. Minority carrier lifetime measurement of the passivated samples has been performed and the analysis shows that success has been achieved in terms of passivation and compared to already existing hydrogen passivation, hydrogen sulfide passivation is actually better. Also the surface passivation by Al_2O_3 helps to increase the lifetime even more after post-annealing and this helps to attain stability for the bulk passivated samples. Minority carrier lifetime is directly related to the internal quantum efficiency of solar cells. Incorporation of this technique in making mc-Si solar cells is supposed to result in higher efficiency cells. Additional research is required in this field for the use of this technique in commercial solar cells.

DEDICATION

To my beloved parents

ACKNOWLEDGMENTS

I would like to express my deepest gratitude to my advisor, Prof. Meng Tao for his motivation and guidance during the research. Right from the very beginning, he tried to take out the best from my efforts and patiently helped me to correct any mistakes I made. This thesis would not be possible without his support. I would also like to thank Prof. Dragica Vasileska and Prof. Michael Goryll for taking out their valuable time for being in my thesis defense committee. I asked for their personal advice and help a number of times during my studies. I am grateful to them for those moments.

I would like to thank Dr. Haifeng Zhang for helping me with the experiments and always inspiring me. I would also like to thank Mr. Wen-Cheng Sung for taking out his time for helping with my experiments. I would also like to thank my research group members: Mr. Laidong Wang, Mr. Woo Shin, Mr. Bin Zhou, Mr. Wen-Hsi Huang and Mr. Mathew Lee for their friendship and support whenever I needed.

I would like to thank Saugata, Hasin and Refat, my current and previous roommates who were more than friends to stand all my faults and to help me in every possible way. Also my heartfelt thanks go to my colleagues and friends of ASU for being available when I needed them most.

Finally, I would like to thank my beloved mother for her outstanding support, sacrifice and well wishes throughout the whole thesis work.

TABLE OF CONTENTS

Page

LIST OF TABLES

Table Page

LIST OF FIGURES

Figure Page

CHAPTER 1

INTRODUCTION

1.1 Energy: World Perspective

Ever-increasing energy demand is a major concern in the current situations of the world. World energy consumption is increasing a lot in the current century and fossil fuel still remains the major source of energy. According to the reports of 2012 from International Energy Agency (IEA), among fall other fossil fuels, coal contributed to more than half of the increased demand of energy [1]. Use of fossil fuel energy increased by more than 23 % from 2000-2008. According to the reports of IEA in 2011, fossil fuel contributed ~ 68% for the total electricity generation in the world [2].

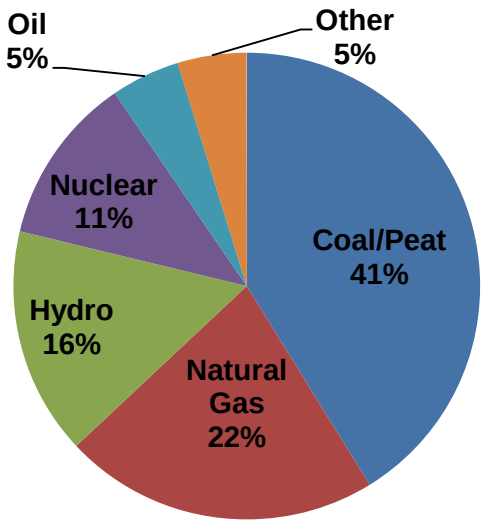

Figure 1.1 World Electricity Generation from Different Fuels [2]

In figure 1.1, other sources mean solar, wind, geo-thermal, bio etc. It can be observed that renewable sources like hydro, solar and others are currently contributing ~21 % of the total generation. Recent Fukushima Daiichi nuclear disaster in 2011 and Chernobyl disaster in 1986 have been the main cause of the end of rapid nuclear power

capacity growth all over the world. After these disasters a number of countries changed their future policy of power generation. But the major threat of global warming still prevails due to the excessive use of fossil fuels. Global warming refers to the increase of average temperature of the air and the earth's surface mainly caused by the intensified greenhouse effect. This leads to the melting of the ice at the north and south poles and thus increasing the height of sea level. Also changes in the current ecosystem and increased heat content of the oceans are the direct results of global warming. Fossil fuel burning for energy production is the main cause of greenhouse effect which results in global warming. So to phase-out fossil fuel, an extensive energy plan is required.

If alternative energy sources have to replace or at least reduce the use of fossil fuels, they need to meet some basic requirements. First of all, these sources must be in large quantities. They also need to be renewable, clean and green; emitting no carbon dioxide (CO_2), sulfur dioxide (SO_2) or nitrogen oxides (NO_x). And most importantly, these sources need to be cheap to compete with fossil fuels. According to Hoffert et al [3], currently the demand is ~15 TW and is predicted to be ~46 TW in 2100. Now this huge demand cannot be met if renewable energy sources cannot contribute a large portion. And among all renewable sources, solar energy is the only source that can meet the requirements stated above. In the next section the prospects of conversion of solar energy to electrical energy have been discussed.

1.2 Photovoltaics as a Source of Energy

In 2006, Lewis and Nocera indicated that only solar energy has the potential to meet the huge future demand [4] forecasted by Hoffert et al as mentioned in the previous section. They argued that although solar energy till date is not even close to $1/10^{th}$

contributor for the current energy demand, the future of solar energy still looks promising. It is the only source that is long lasting (billions of years), geographically distributed and only it can offer even more than the requirement of 46 TW with ~600 TW of probable practical generation [4]. Actually, solar energy can provide more energy in one hour to the earth than 1 year demand of the total energy of the world.

Solar energy can be converted to useful energy through 3 mediums: Solar to thermal, electricity and chemical energy. Each of these processes follows the same sequence- capture, conversion and storage [5]. Now solar to electricity conversion is known as the 'Photovoltaic effect'. Solar cells are also called photovoltaic (PV) cells. The explanation of this conversion relies on the basics of quantum theory.

Becquerel first discovered the PV effect in 1839 [6]. His experimental set up had a silver chloride (AgCl) electrode and a platinum (Pt) electrode in acidic solution [5]. He observed a voltage drop as light shone on the AgCl electrode. The first solar cell was invented by Charles Fritts in 1883 [7] who used selenium wafers with very thin layer of gold to form metal-semiconductor junction. The efficiency was <1% then. Russell Ohl invented the first silicon solar cell in 1941 [8] and it readily proved to be a better semiconductor. To-date silicon solar cells are the most widely used cells. In 1954, Pearson, Fuller and Chapin invented Si solar cell with ~6% efficiency [9]. They were able to make an array of cells and thus the first solar panel. In 1985, solar cell efficiency crossed ~20% efficiency [10]. Gallium Arsenide (GaAs) solar cells were also fabricated with higher efficiency in 1980s.

Currently, a number of commercially available cell technologies are there which include wafer silicon (both crystalline and multicrystalline) solar cells, thin film cadmium

telluride (CdTe) cells, thin film silicon cells (amorphous or microcrystalline), thin film copper indium gallium selenide (CIGS) cells, III-V compound semiconductor multi-junction tandem cells etc. Currently developing solar cell technologies include dye-sensitized solar cells, perovskite cells, organic solar cells, quantum dot cells and thin film copper zinc tin selenide sulfide (CZTSS) cells. The current record of laboratory efficiency for different solar cell technologies has been shown in figure 1.2.

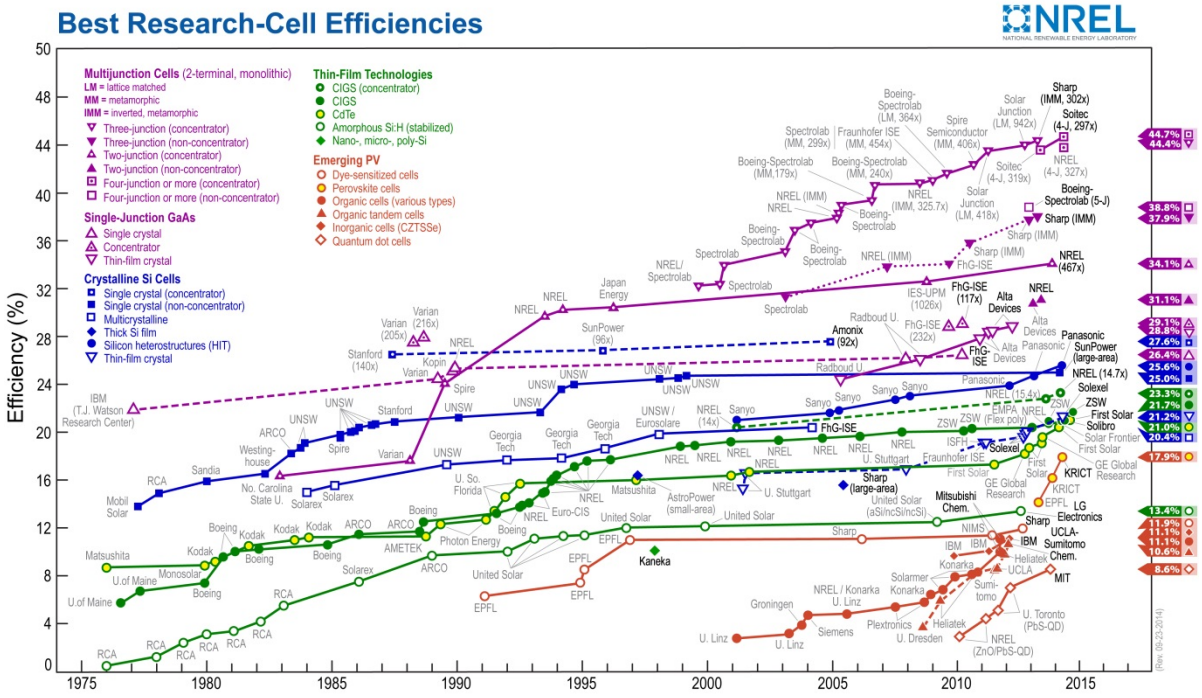

Figure 1.2 Record of Best Research Cell Efficiency [11]

Solar cells have been in use for a number of decades now. Successful use of solar cells includes earth orbiting satellites, hand-held calculators and water-pumping applications. U.S. Department of Energy (DOE) started funding PV R&D applications right from its start in 1976 [5]. Solar cell manufacturing had a vital and rapid growth for the last 10 to 20 years. Annual production of solar module has increased ~10 times every

decade. In figure 1.3, annual production of PV power vs. time is shown for 1988-2003. Total PV cell production increased from 10 MW_p/year (1980) to 1200 MW_p/year (2004).

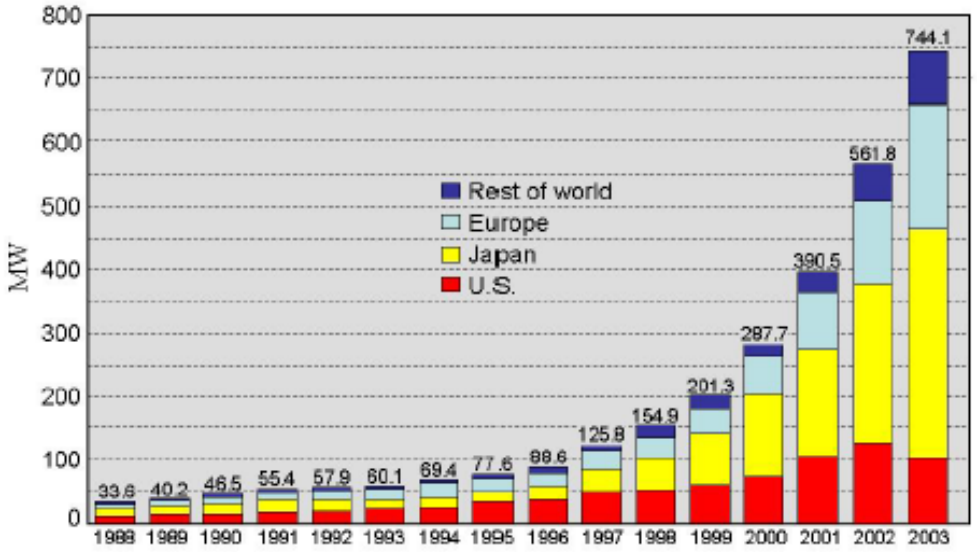

Figure 1.3 World PV Cell/module Production from 1988 to 2003 (in MW_p) [5]

Among all the cells deployed, ~85% comes from the wafer silicon (c-Si and mc-Si) and mc-Si contributes to ~53% of the total PV market. As silicon is the second most earth abundant element, its availability is handy for the current and future use for PV.

1.3 Silicon Solar Cells: Defects and Passivation

Silicon is an indirect bandgap semiconductor. Recombination losses in it occur largely via defect levels. These defects could be inside the volume (at the bulk) or at the surface of the wafer. Also there can be extrinsic defects like the processing related defects. Depending on the silicon growth method, the density of extrinsic defects could be high or low. The surface is the most vulnerable part to disturbance of the symmetry of the crystal lattice. Defects exist at the surface due to the dangling bonds. These are the main reasons of surface recombination losses which affect the efficiency of solar cells [13].

In multicrystalline silicon (which is grown normally by casting process), a large amount of grain boundaries can be induced. These grain boundaries (shown in fig 1.4) act as high localized regions of recombination as they introduce extra defect levels into the bandgap. This results in the decrease of minority carrier lifetime. Also grain boundaries block carrier flows and provide shunt paths and thus decrease the efficiency of the solar cells [13, 14].

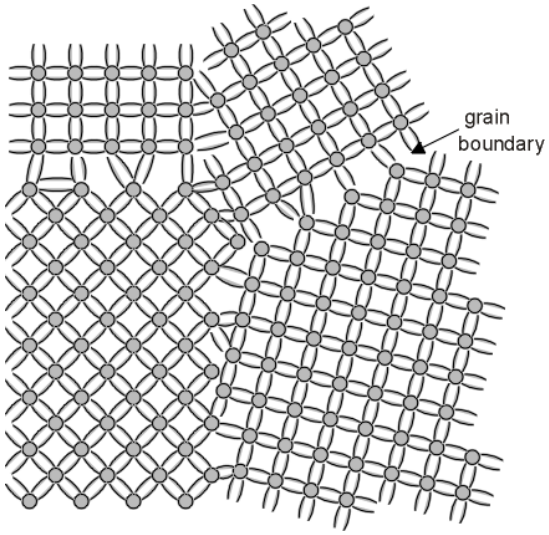

Figure 1.4 Grain Boundary in Multicrystalline Silicon [13]

From the above analysis it is clear that it is really important to find out methods for dealing with the defects and impurities for both c-Si and mc-Si. To take care of the dangling bonds and defects, ‘passivation’ is a very useful technique which can take care of the defects and thus keep surface recombination as low as possible. Aberle argues that in case of solar cells, this passivation needs to have long term stability [12]. Surface passivation and bulk passivation both are important research topics which lead to the rise of efficiency [12-15].

In this research work, the target was to design a reliable and stable technique of grain boundary passivation for mc-Si samples using hydrogen sulfide. Additionally, a compatible surface passivation to accompany the bulk passivation was necessary to achieve high lifetime gain compared to unpassivated samples. The proposed technique is new and therefore introduces a lot of questions regarding effectiveness, comparison to the existing techniques, stability etc. In the next chapters the answers to these questions have been described step by step.

1.4 Thesis Outline

This thesis has been divided into 5 chapters including this one. In chapter 2 the different aspects of bulk passivation has been described for achieving a thorough conception. The dependence of electrical and photovoltaic properties on the grain size has been stated in details. Currently a number of bulk passivation techniques are being used in the industry and research labs. This chapter also covers those along with significant findings which could be helpful for the design of experiment.

In chapter 3 a new set of experimental procedures designed for grain boundary passivation by hydrogen sulfide have been described. A detailed explanation of the chosen material, equipment and components used in the lab has been mentioned with a step by step walkthrough of the procedure. Along with hydrogen sulfide passivation, for the sake of comparison and other reasons, hydrogen passivation also had to be performed by forming gas annealing (FGA). The procedures for that have also been described.

In chapter 4 the results of the experiments (performed according to the procedures of chapter 3) have been analyzed and explained with the help of figures and tables. The

quality of passivation and degree of improvement through passivation and annealing has been examined. The stability of the passivation also has been tested.

In chapter 5 a comprehensive summary of the work has been stated. Key points and achievements of this research have also been discussed. Also the future scope of research work in this sector has been mentioned.

CHAPTER 2

REVIEW OF BULK PASSIVATION

2.1 Introduction

Multicrystalline Silicon (mc-Si) is considered to have a great potential for large scale photovoltaic application due to the very fact that it can save a lot of complex steps which are necessary for the growth of single crystal silicon. Meanwhile, it still has the positive aspects of c-Si like abundance on the earth and stability [16]. Currently, the efficiency of mc-Si solar cells is less than 15% in industrial solar cells and the best in the research labs is ~20.4% [11], which is a bit less compared to c-Si which demonstrated ~26.4% efficiency in the research labs [11]. This difference in efficiency is mainly contributed by a number of factors.

The first negative effect from grain boundaries of mc-Si is the fact that these grain regions possess attractive potential for photo generated minority carriers. Also the carriers are exposed to a very high concentration of recombination centers if they are trapped at right on the middle of the boundaries [14]. Another negative effect caused by the grain boundaries is the shunting action which overlaps p-n junctions. As a result, the open circuit voltage (OC voltage) and the fill factor of the device go down.

In this chapter, an overview of the currently existing bulk passivation techniques has been provided. The chapter starts with the discussion on the theory of the electric and photovoltaic properties of mc-Si. Then a review of the current and previous techniques on bulk passivation has been included. The target is to pick up key points of a passivation procedure and the characteristics improvement expected after passivation. This

theoretical study sets the tomb for the design of the experimental procedures followed in the next chapter.

2.2 Effect of Grain Size on Different Properties

Photovoltaic properties vary quite a lot in mc-Si devices. Ghosh et al argues that this wide variation can be explained with the help of effects grain size variation in the devices [16]. Grain boundaries can be situated at varied number of sites a solar cell. There are 3 types of grain boundaries:

- Type 1: these grain boundaries are along the columns
- Type 2: these are deep into the bulk of the crystal
- Type 3: these are in the p-n junction region

Only the effects of type 1 were taken into account previously while making the estimation of short-circuit photocurrent and as a result, the number from theoretical calculations and practical experiments tended to have some difference. After considering the contribution from type 2 and type 3, this gap decreases a lot. Grain boundaries essentially are the “traps” which also act as recombination centers increasing the surface recombination velocity [13]. A number of properties have been described below which have correlation with grain size.

(i) Carrier Concentration and Mobility

Concentration of doping is a quintessential factor for the determination of performance in solar cells. For both c-Si and mc-Si, the change in the mobility and resistivity with respect to the doping is not same. The mobility of majority carrier varies with the change in doping concentration. For both p and n-type majority carriers in mc-Si, mobility first goes down with the increase in doping. After reaching a certain point, it

again goes up. So there is a change in the sign of the slope for the curve. Now as the mobility of the majority carrier reaches its minimal value, a sharp increment in free carrier is obvious.

The doping concentration at which both these happen has been formulated by [16] to be as follows:

$$N_d \approx \frac{10^{12}}{d}$$

Here, N_d is the doping concentration and d is the grain size in cm. The number 10^{12} is due to the factor of trap sites in grains. A number of independent studies [18-20] found that magnitude of grain boundary traps inside $\pm$ 0.02 eV of the midgap was almost 10^{12} cm^{-2}.

Correlation between resistivity and doping is again different in c-Si and mc-Si. For c-Si the resistivity decreases linearly with almost a constant slope for both n and p-type. For n type mc-Si, the resistivity decreases very fast at lower doping but becomes steady after sometime and in line with n type c-Si. For p-type mc-Si the resistivity starts at a very high value compared to c-Si and then starts decreasing with doping. After the doping was more than 10^{18} cm^{-3} there was a sharp fall in the resistivity [16, 18].

(ii) Lifetime

A common procedure for lifetime measurement is photoconductance decay technique and according to it, the effective lifetime depends both on bulk lifetime and surface lifetime [12]. It is given by the following formula:

$$\frac{1}{\tau_{\mathrm{eff}}} = \frac{1}{\tau_{\mathrm{b}}} + \frac{1}{\tau_{\mathrm{s}}} \quad \ldots \quad (2.1)$$

where τ_{b} is the bulk lifetime and τ_{s} is the surface lifetime. Again τ_{b} is represented as a function of SRH, auger and radiative recombination [13].

$$\frac{1}{\tau_{bulk}} = \frac{1}{\tau_{\mathrm{SRH}}} + \frac{1}{\tau_{\mathrm{Auger}}} + \frac{1}{\tau_{\mathrm{rad}}} \ldots \qquad (2.2)$$

According to the equation, bulk lifetime is influenced by both intrinsic and extrinsic recombination. As silicon is not a direct bandgap material, radiative or band-to-band recombination is minimum for it. Auger recombination dominates lifetime in case of very high carrier concentrations or high injection cases. With the increase in doping, τ_{Auger} decreases sharply and the effective lifetime goes down [13]

Surface lifetime mostly depends on the characteristics of the surface. If the surface has areas of defects and the lattice is disrupted, another kind of recombination called surface recombination comes into play. This surface recombination is generally high in case of solar cells if not taken care of in a proper manner. Due to the presence of the dangling bonds at the surface and high recombination rate, the close-by area of the surface depletes of minority carriers. This results in a flow of carriers from the nearby high concentration areas due to the diffusion effect and the recombination rate increases [12,13]. So it can be said that this rate of recombination can be controlled by the movement of minority carriers towards the surface. To take care of the dangling bonds at the surface and hence to reduce surface recombination rate, a layer is grown on top of the semiconductor surface which ties up the dangling bonds. As a result, these sites cannot work as surface recombination sites anymore. A number of passivation techniques have been in use for long time. In fact, surface passivation is one of the major research areas in the solar cells as the efficiency improvement due to this is quite considerable.

Now in equation 2.1, for a symmetrically passivated wafer, the surface recombination velocity is assumed to be pretty low. And 2.1 is rewritten as [12, 21]

$$\frac{1}{\tau_{\text{eff}}} = \frac{1}{\tau_{\text{bulk}}} + \frac{2S_{\text{eff}}}{W} \ldots \quad (2.3)$$

Here, W is wafer thickness and S_{eff} is effective surface recombination velocity. Normally the value of S is on the order of 10^7 cms^{-1} for a surface which has infinite number of fast recombination [13]. For a well passivated surface like used in equation 2.3, S_{eff} is lower than 250 cms^{-1}.

Shockley derived equations relating τ_s and the cross-sectional dimensions for a rectangular filament [22]

$$\frac{1}{\tau_s} = \frac{1}{4}\pi^2 D \left(\frac{1}{B^2} + \frac{1}{C^2}\right) \quad \text{when } s \to \infty \quad (2.4)$$

$$\text{and} \quad \frac{1}{\tau_s} = \text{s} \left(\frac{1}{B} + \frac{1}{C}\right) \quad \text{when } s \to 0 \quad (2.5)$$

Here D = diffusivity. Lorefski went further with the calculations [16] and derived the following equation:

$$\frac{1}{\tau_s} = \frac{D\pi}{2R^2} \text{ for } s \to \infty \quad (2.6)$$

where R is the radius of the cylinder. Later Card and Yang derived another formula [23] where they define effective lifetime as

$$\tau_{\text{eff}} = \frac{2d \exp(-qV_d/kT)}{3\,\sigma v N_{\text{is}}\,(E_{\text{fn}} - E_{\text{fp}})} \quad (2.7)$$

Here,

v = carrier thermal velocity

V_d = height of the diffusion potential at the grain boundaries

N_{is} = density of interface

σ = capture cross-section

d = dimension of the assumed cube

E_{fn} and E_{fp} = quasi-fermi levels for electrons and holes.

Ghosh et al. obtained a good estimate of the lifetime [16] even after neglecting the term for the diffusion potential at the grain boundary. They postulated that the following equation is enough for τ_{eff} calculation:

$$\tau_{eff} \approx \frac{1}{\sigma v N_{sr}} \quad \ldots (2.8)$$

Here, they introduced another parameter N_{sr} to denote effective density of recombination centers. The assumption was that the sites for recombination are evenly distributed all over the bulk of the material and as a result, N_{sr} has a linear relationship with the actual number of recombination sites. For a cubic shaped crystal structure [16],

$$N_{sr} = \frac{6\,N_{ss}}{d} \quad \ldots (2.9)$$

Here, density of recombination centers is denoted by N_{ss}. So 2.8 becomes

$$\tau_{eff} \approx \frac{d}{6\sigma v N_{ss}} \quad \ldots (2.10)$$

This model is acclaimed to have been able to match with the experimental results and also explain the observed parameters associated.

2.3 Grain Boundary Passivation Methods

From the previous section, the basic idea behind the grain boundary and its influence on device parameters should be obvious. To take care of these effects, a number of passivation methods have been in use for long time. In this section, different grain

boundary passivation technologies have been deliberated to have a strong background of the prevailing technology that helped to design the experimental procedures which have been described later.

(i) Passivation Using Hydrogen Plasma

This is one of the earliest methods for bulk passivation of mc-Si that was used by Seager and Ginley [14]. In their experiments, they successfully introduced hydrogen plasma in mc-Si which proved to be effective at the removal of grain boundary or "in-gap" states in the material. In another paper, Seager and Castner measured the zero-bias resistance [19] of the depletion layers near the grain boundaries in "neutron transmutation" doped mc-Si. They established a model that describes the relationship between the doping dependence of zero-bias resistance with the density of electron states located near the boundaries.

The zero-bias resistance evidently changed exponentially with the change in the barrier height. Low voltage experiment on each grain boundary is extremely sensitive for quantification of any effect due to any chemical change. So introduction of hydrogen in the boundary regions in this environment was really a challenging task.

For the experiments of Seagar et al. the grain sizes varied from 200 to 500 μm and the material was "single-float-zone-pass semiconductor device grade silicon". Annealing was performed to take care of the damage caused by radiation and annealing was done in vacuum at 750 °C for 40 minutes. Gas treatments were performed in a quartz vessel connected to a high vacuum system. Excitation of plasmas was performed by a metal band connected to a Tesla coil supplying voltage at 1 to 5 kV. The experiment is typically performed at 0.1 torr [14].

With the obtained results they prepared a graph showing the conductance vs 1/T characteristics for both virgin samples and hydrogenated samples. Now from the graphs, it was obvious that the introduction of hydrogen increases the conductance at all the temperatures. As the temperature increased, the conductance went up. This happened due to fact that introduction of hydrogen in the bulk decreases the effective resistivity as the number of recombination sites goes down.

The space-charge regions near the grain boundaries were wide enough and as a result it was assumed that the transport is mainly due to the thermal emission current [14, 19]. Activation energy E_A of the zero-bias resistance is associated with Φ_B (conduction band bending)*:*

$$E_A = \Phi_B - \frac{T\partial\Phi_B}{\partial T} \quad (2.11)$$

According to the claims of [19], E_A does not depend on temperature when the range is 270 to 370 K. From the observations of Seager et al, if the density of grain boundary states would decreases at or near the Fermi level, it would result in a decrement of Φ_B and from the equation 2.11 it can be said that E_A would also lower down. Among some other results, there were some significant observations made by Seager et al which are as follows:

1. Although hydrogen plasmas had been proved to be useful at removal of grain boundary recombination centers (as observed from the conductance vs 1/T), other gases like oxygen, sulfur hexafluoride (SF_6) and nitrogen have not been able to do so. For these, they actually decreased the conductance.
2. Even hydrogen in molecule form was not good enough for this treatment.

3. The hydrogenated samples were stable enough and show a stable conductance around 300K showing that this technique was reliable.
4. Plasma treatment did not change the other characteristics of the bulk silicon as the diffusion was low in these rang of temperature.

(ii) Passivation Using Low Energy Hydrogen Ion Implantation

A number of papers discussed about the various aspects of this passivation technique [24-26]. Through these papers, it has been established that ion implantation at low energy can improve the electrical properties of mc-Si and thus increase the efficiency of solar cells. Using a Kaufman-type ion source or similar equipment was considered to be the best approach as the processing time reduces a lot by this. Muller et al. proposed a method which did not require magnet and highly stabilized power supply and hence was more cost effective [24].

A number of analysis methods like SIMS, RBS, reflectivity, ellipsometry were performed on p-type wafers. Also C-V, I-V characteristics, DLTS were performed before starting the experiment to compare the results before and after the experiment [24, 27]. The described ion source had extraction energy in between 0.1 to 1 keV and the source had a post-acceleration electrode. For generation of electrons, the ion source had a tungsten filament. A magnetic coil helped to raise the ionization of the used gas.

After the experiments both macroscopic and microscopic analysis were done on the samples. Distribution of hydrogen for different temperature and different ion source energy were plotted. Also hydrogen concentration vs penetration and time of irradiation were plotted. Important parameters for solar cell like reflectivity and absorption coefficients were also measured for virgin mc-Si, hydrogenated mc-Si and single c-Si to

compare the quality of passivation. Muller et al showed that reflectivity increases for hydrogenated sample for a broad wavelength range of 250 to 800 nm [24]. Also for the case of absorption coefficient they report an increase for the wavelength spectrum of 0.3-1.1 μm. This clearly helped to increase the internal quantum efficiency of the hydrogenated mc-Si samples compared to the virgin mc-Si samples. Microscopic analysis was performed to find out the defects caused by the bombardment of ions and the amount of damage of structure. For example, C-V curve showed irregular effects around the surface up to a distance proportional to the hydrogen penetration [27]. They also reported that annealing at 700 °C for 30 minutes was enough to retain the original curve.

From another experiment, it was found that the dominant peak could also act like a trap or recombination center for majority carriers which was actually another defect that was caused by ion bombardment. Again this could be removed by annealing at just lower than 400°C. I-V characterization was done for 2 different sets of mc-Si silicon samples in dark and AM1 condition. Open circuit voltage (V_{OC}) and Short circuit current (I_{SC}) were characterized for hydrogenated mc-Si. The experiments showed improvement in both of them at a certain implant dose and temperature. For dark I-V, a small improvement of junction quality was reported [24]. For both kind of mc-Si samples used, the best conditions for achieving higher fill factor and efficiency are reported. Spectral response for different sample sizes were measured and internal quantum efficiency for different wavelengths were measured which shows improvement after hydrogenation [28].

Stability is the only concern that comes into the picture here. After the experiments were repeated over time, there were some degradation both in V_{OC} and I_{SC} as

they tend to decrease a certain amount very quickly. The change was not exponential and the values were almost fixed after a certain number of days.

(iii) Passivation with Al Treatment on Back, Forming Gas Anneal and Oxide Passivation

This process is followed for a number of different cases including edge-defined film-fed grown (EFG) mc-Si. EFG Si has a high grain size with the average from a few mm to ~1cm [29]. Having so large grains, the samples tend to have lots of dislocations, twin boundaries and impurities. Sana et al proposed a process that combined the gettering effect of Aluminum on the back, oxide passivation on the front surface and forming gas annealing (FGA) [29]. They reported an efficiency change from 7.8 to 14.1%.

p^+ back surface field was formed by Al treatment by evaporating 1 µm Al on the back and then a drive-in at 850 °C for 35 min. surface passivation was achieved by oxide formation and that was performed simultaneously during the drive-in of Al. According to Sana et al [29, 30], this helped to make the process easier and cheaper. To differentiate between the processes, some samples did not undergo Al diffusion on the back and some did not go through FGA. For the cells without All BSF, Al back contact was used.

FGA was performed for 2 hours at 400 °C. Forming gas contained 10% hydrogen. After this, 2 drive-ins were performed again at 400 °C using FGA and each of them lasted for 45 min. The sample set that did not go through annealing, were annealed in nitrogen ambient for same amount of time (2 hours) and went through similar drive in for 45 min with nitrogen.

After following the procedure mentioned above, the authors achieved a set of samples to compare and derv the effect of each and every step. Those were

- Samples with no oxide, no Al BSF, no FGA

- Oxide, no Al BSF, no FGA
- Oxide, Al BSF but no FGA
- Oxide, Al BSF and FGA

Now with all these samples a number of characterizations like measurement of internal quantum efficiency (IQE), V_{OC}, Short circuit current density (J_{SC}), Fill factor, Series resistance, shunt resistance, lifetime and diffusion length were performed.

Even for large grain cells like EFG had an improvement of IQE which were visible just after oxide passivation as oxide passivation on the surface had already been proved to be the best among surface passivation techniques [31]. Sana et al. reported in their paper that Al BSF also improved the IQE further after oxide passivation which meant that the effects were being added to each other. Also Al BSF increased $V_{OC,}$ J_{SC}, diffusion length.

Hydrogen passivation of bulk was already well established and in this case FGA was performing as the carrier gas of monoatomic hydrogen and thus improving the IQE. FGA was reported to be very compatible for solar cell fabrication and used as a routine procedure for MOS devices for decreasing the interface density of Si-SiO_2 [29, 30].

Another set of experiment was performed to find out any correlation between Al BSF and FGA. So two sets of samples were prepared- one with FGA and Al BSF (through diffusion) and the other set with FGA only and Al just as back contact. Both had oxide passivation. For the 2^{nd} set, there was an improvement of IQE compared to oxide passivated sample. But when Al BSF was used with FGA, there was further improvement which could be only explained by the fact that Al BSF helps to generate additional

atomic hydrogen which in turns achieves more bulk passivation and results in higher IQE [29]. Thus this method stands as one of the standard methods for passivation.

(iv) Passivation using Hydrogen Rich Amorphous Silicon Nitride (SiN_x:H)

Amorphous SiN_x:H is right now playing a very important role for the fabrication of mc-Si solar cells. Its significance is mainly due to 3 reasons [31-36]

- SiN_x works as the antireflection coating which is a must in a solar cell. The refractive index of the layer can be varied by changing the Si:N ratio over a wide range of 1.9 to 2.5 [34] which is required for almost every kind of cells.
- SiN_x itself is a good surface passivation material. And it has the added benefit of saving another layer or process cost as it is already used for the antireflection coating. Although nitride passivation is not as good as oxide passivation (which is the best for surface passivation) [12, 31], still it is the most widely used technique.
- SiN_x:H can be also used for hydrogenation of the bulk if a short thermal process is introduced and thus reducing the number of defects and impurities in the bulk.

For the deposition processes of SiN_x, a number of processes have been described in [31-35]. The most effective of them are the various chemical vapor deposition processes like atmospheric pressure CVD (APCVD), low pressure CVD (LPCVD), plasma enhanced CVD (PECVD). These processes use silane (SiH_4), ammonia (NH_3) or nitrogen as reactant gases. PECVD has some benefits compared to LPCVD and APCVD. Those are as follows:

- Deposition rate is higher for PECVD [34,35]
- Offers lower processing temperature (500 °C) compared to APCVD (700-900 °C) and LPCVD (750 °C) [35]

- Better antireflection coating as it has higher tuning range of refractive index of SiN_x by controlling Si:N
- Better quality surface and bulk passivation from PECVD nitride [33-35]

J. Hanoka et al. made important contributions regarding the use of SiN_x passivation and its application as passivation material [35,36]. Now there are 2 different methods of PECVD- direct and remote PECVD [35].

Direct PECVD

All the gases (SiH_4, NH_3, N_2) are injected directly among the electrodes and the set electromagnetic field excites them. Si substrates are placed within the plasma. Direct plasma excitation is performed by the generator. 3 frequency ranges can be used: Low (10 – 500 kHz), High (13.56 MHz) or very high (30-100 MHz). Low frequency can cause surface damage as a result of heavy ion bombardment and result in worse passivation [12]. Sometimes damages can be helpful for bulk passivation [37].

Remote PECVD

Plasma excitation performed outside the chamber; usually microwaves are used. Normally, NH_3 or N_2/H_2 are "excited and directed onto" a substrate. SiH_4 is directly injected into the chamber and there it gets dissociated by the atomic hydrogen. For remote PECVD, rate of deposition is higher and also it comes with a surface damage free passivation system. Main disadvantage is that remote PECVD might not be the best option for bulk passivation as there was no damage done by the plasmas [35].

For achieving higher bulk passivation, direct PECVD also incorporated a heat treatment which frees up hydrogen from Si and N and diffuses into the layers of mc-Si and in the process bind itself with the dangling bonds and thus help to increase the quality

of passivation [35]. This process is called “firing through” in which the front cell contacts of Silver (Ag) are fired through the layer of nitride. Good contact between emitter and front contact is achieved in this process which helps to achieve higher fill factor. The passivation quality of bulk from depends on the defect states in the used material. If there are more defect states, the passivation is inherently better [34,35]. Duerinchx et al. described some more benefits of the firing through process:

- *Emitter passivation*: During the ion bombardment, the surface is damaged which is annealed during this treatment during which nitride passivates the emitter.
- *Diffusion barrier:* Nitride layer works as diffusion barrier which prevents “metal spikes” deep into the bulk and thus helps to decrease any shunting action
- *Al-BSF formation:* Creates the necessary field for an “in-situ” Al-BSF formation for no extra process and cost. And the Nitride layer works as diffusion barrier which prevents “metal spikes” deep into the bulk and thus helps to decrease any shunting action

From all these discussions, the reasons behind the popularity of amorphous SiN_x:H is clear. If any new technique has to compete with the existing ones, it certainly has to go through the testing procedure before being recognized as a passivation source.

2.4 Conclusion

After the thorough study made in this chapter, a general idea of bulk passivation technique is now clear. The ideas are very important for designing a new experiment because a number of key points have to be taken care of for bulk passivation of mc-Si samples and also to compare the new technique with the existing techniques.

CHAPTER 3

DESIGN OF EXPERIMENTS

3.1 Introduction

A number of popular and well established techniques for bulk or grain boundary passivation have been described in the previous chapter. From the understanding, it is obvious that the mc-Si solar cells are still far away even from c-Si solar cells in terms of efficiency. So to find out new, feasible and reliable passivation techniques is a continuous journey in this field. The most challenging part is to find out commercially usable one with higher lifetime and efficiency. Theoretical studies and practical experiments are being continued on alternative techniques of surface passivation and bulk passivation which are to be incorporated with solar cells in the near future.

In this chapter, a new grain boundary passivation technique is proposed. The design of the experimental procedures has been described step by step. The equipment used in the lab and the set of conditions followed are also mentioned. The results and analysis of experiments have been detailed in the next chapter.

3.2 Material Selection for Bulk Passivation

Choice of a new bulk passivation technique starts with the selection of the right material. A number of important considerations have to be made for this. For the proposed grain boundary passivation technique, a novel material has been proposed and Hydrogen sulfide (H_2S) has been chosen. To the best of the knowledge of the authors, hydrogen sulfide has not been used for bulk or grain boundary passivation of mc-Si. The initial reasons behind its choice and the ideas proposed for the passivation and then the details of experiment have been explained here.

(i) Success in Surface Passivation

For a number of years, use of sulfur as a surface passivation of crystalline silicon (c-Si) was proved to be very successful by the research of M. Tao and his group [38-41]. Sulfur passivation using a solution as a sulfur source like ammonium sulfide $(NH_4)_2S$ has been studied [39]. They were able to reduce the number of density states by more than one order of magnitude. This change was visible from the barrier height of Al and Si. For Al and n-type Si (100), they reported < 0.11 eV which was way less than 0.56 eV of unpassivated samples. For Al and p-type Si (100), they reported a record of 1.10 eV as seen from the I-V and C-V characterization whereas for unpassivated samples it was 0.66 eV. Also for the higher work function metal Ni, they achieved a barrier height of 0.75 eV with n-Si (100) and 0.51 eV with p-Si (for non passivated 0.61 eV and 0.54 eV respectively).

Later, H. Zhang et al under M. Tao demonstrated that sulfur could be used also from a gas source like hydrogen sulfide for surface passivation. They reported a reliable and stable surface passivation from sulfur using chemical vapor deposition based technique. For Al and n-Si (100) the reported barrier height was less than 0.08 eV from both I-V and C-V characterization [41]. For Al and p-Si, the barrier height from C-V was 1.14 eV and ~0.77 eV from I-V curve. The difference of these values was caused by image force lowering of barrier and edge leakage current [41].

Experiments on the improvement of surface passivation of mc-Si were conducted in the lab with ex-situ and in-situ cleaning with a 2 step passivation recipe. But the success on mc-Si largely depends on the large rate of recombination that happens in the grain boundary regions of mc-Si. So no significant results were reported from only the

surface passivation of mc-Si. To minimize the recombination rate of minority carriers in the grain boundaries hydrogen sulfide diffusion was a choice for which the experimental design could be easily set up given that the lab was already prepared with necessary equipment for surface passivation and using hydrogen sulfide for that. Also the comparison between the quality of bulk passivation by hydrogen and H_2S could be easily done as hydrogen was already being used as a cleaning step for surface passivation.

(ii) Benefits as an Element

For surface passivation, especially valance mending passivation (VMP), some guidelines were proposed by Kaxiras [43]. But for grain boundary passivation there are no such guidelines. One guideline for VMP mentioned that the covalent radius of the adsorbate and silicon should be very close. Now even for bulk passivation, if this holds true, then there is supposed to be a stronger bond between the foreign particle used and the silicon atoms in the bulk. For hydrogen, the covalent radius is 32 pm, 111 pm for Si and 105 pm for sulfur [44]. So sulfur should be a good match for Silicon if it can be diffused into the bulk.

Another advantage of sulfur is that it is heavier as its atomic mass is higher. So the desorption rate of sulfur would be much lower than hydrogen. Also sulfur has valency of 2 meaning that one atom can make 2 covalent bonds and take care of 2 dangling bond whereas hydrogen has valency of 1 which means each atom of hydrogen can take care of one dangling bond at a time.

(iii) Combined Effect from Hydrogen and Sulfur

As mentioned in chapter 2, all the current and previous bulk passivation techniques used hydrogen to passivate the grain boundary regions. In the proposed work,

hydrogen sulfide use helps to take the advantage of both hydrogen and sulfur at the same time. As evident from the periodic table, hydrogen is much smaller in size compared to sulfur. If the grain boundary regions are big enough, it can be a place for sulfur item to fit and stay more easily than hydrogen. The covalent bond is supposed to be stronger between silicon and sulfur compared to silicon and hydrogen.

(iv) A Compatible Surface Passivation with Bulk Passivation

After studying the bulk passivation techniques thoroughly, the importance of the surface passivation becomes obvious. If the bulk passivation is not accompanied by a compatible and reliable surface passivation simultaneously, the increase of the internal quantum efficiency is almost always undetected. And measurement of lifetime and its degree of improvement can be only detected only when there is no surface recombination. For example, bulk hydrogen passivation is almost always incorporated with nitride passivation or oxide passivation. This oxide or nitride passivates the surface and makes any change in the improvement in the bulk detectable. For the proposed technique, the order of merit of passivation quality is lifetime measurement for which a stable surface passivation is a must. For this, Aluminum oxide (Al_2O_3) is used which is already acknowledged as one of the best surface passivation techniques in use.

3.3 Experimental Set up and Equipment

Before going to the details of the experiment, choice of equipment and their role in the experiment are very important to understand the recipe and the results.

(i) Diffusion Furnace

The diffusion furnace from MTI corp. consists of a quartz tube which is 600 mm long, has the outer diameter (OD) of 50 mm and inner diameter (ID) of 43 mm. The

temperature can be set up according to the requirement for specific duration. Maximum temperature rating is 1100 °C. The tube can work properly in low pressure conditions.

(ii) Quartz Rod

Loading and unloading the sample inside the tube furnace was an issue, especially unloading the sample from the middle of a quite long quartz tube (as mentioned- the total length is 600 mm) was really tricky. For this purpose, a quartz rod is used. Now this rod was designed with customization specifically for this experiment. The rod is almost 1′-5″ long and the diameter is 1/8″. The front end is divided in two branches which made it look like "Y" in which the tail of the Y is the length of the rod. Now the distance between the heads of the branches (that looked like "V") is ¾″ to make it easily movable inside the tube without touching the metal covers. Also this part was flattened after polishing so that the samples could be placed on this flat surface for loading and unloading. Also the thickness in that part was reduced for making it useful for unloading the sample. So during unloading, the rod's V shaped branches can easily go under the samples that are marginally smaller than the ID of the metal outer rings of the furnace.

(iii) Vacuum Pump, Gauge and Set of valves

Pfeiffer Vacuum facility (Model: HiCube 80 Eco) is used in the lab to control the pressure in the furnace. The display and control unit is easier to operate. The system is set up with a number of flanges and connectors and valves to operate at the exact parameters and conditions. The pump is connected through flexible tubes, flanges and connectors with the tube furnace.

A full range composite Pfeiffer vacuum gauge is connected with the pump which is supposed to give correct data in the range of 10^{-8} to 100 mbar with $\pm$5 % accuaracy

and up to 1000 mbar with $\pm$30 % accuracy. But the problem with the gauge is that it is unable to detect correct pressure after it goes above 10^{-1} mbar as the pirani gauge used in this is not reliable for high range of pressure. But for the designed experiment, at least atmospheric pressure is needed to be measured accurately. So an extra pressure gauge had to be introduced.

(iv) Capacitance Manometer

To measure the pressure in the high range (from 0 to 1000 torr) correctly, a capacitance manometer from Setra (Model 730) is used. This model is very reliable with fast response time, low noise and quick return to zero. And with an accuracy of $\pm$ 0.5% it is the best fit for the purpose. Customized connection for this was ordered to minimize number of connection so that no inaccuracy resulted due to pressure lost in those parts.

(v) Pressure Display Unit

The composite pressure gauge from Pfeiffer needed no extra display as it is connected to the vacuum pump directly and the pressure is displayed in the pump's display unit. But for the capacitance manometer, an extra display unit was needed. Terranova 809 from Duniway Stockroom Corp. is used for this display.

During the installation of the capacitance manometer and the display unit, care was taken to set the calibrations right. Both the zero levels were set properly and atmospheric pressure was tested on them. After the initial set up, no further modification is necessary at any step for these items during the experiment.

(vi) Hydrogen Sulfide Gas source

Hydrogen sulfide gas is flown into the diffusion furnace from a gas cylinder kept in a separate room just adjacent to the lab. The gas flow into the lab system is controlled

by 2 step valve control in the cylinder room along with digital control. All these are for safety measures in the lab to ensure proper environment for safe, sound and reliable operation. The exhaust pressure of the gas from the cylinder is almost 20 – 25 PSI. The gas flows through coaxial lines in which the jacket is always full with N_2. Even the pressure of this N_2 is always kept over a limit of 40 PSI which is another safety measure to prevent any disaster in case of any accidental leak in the coaxial line.

(vii) Pressure Control Valves

After the gas flew into the lab from the cylinder through the coaxial line, it had to go through 2 different control valves before the diffusion furnace. The first valve is a diaphragm valve from Swagelock which could isolate the cylinder from the experimental set up. This is a quarter turn actuation valve which is just like a switch for controlling the gas flow. The handle shape provided indication of 'open' and 'closed' position.

The second valve after the isolation valve is a Bellow-sealed metering valve which is used to fine tune the flow rate of the gas which would go into the diffusion furnace. The handle of the valve could measure 0.001 inch turn and total 6 turns are needed to open the valve to the maximum flow rate. The flow rate (C_v) for the valve could be controlled even lower than 0.005 and as a result pressure fine tuning is very satisfactory.

(viii) Scrubber

The exhaust hydrogen sulfide gas after the experiment from the vacuum pump is flown into a scrubber. The scrubber is a set up for taking care of the toxic hydrogen sulfide by mixing it with water. Water is flown into the system from the utility. A separate control system is set up for the scrubber to operate correctly. Before running any

diffusion experiment, the scrubber control is turned on to make the system ready for receiving exhaust gas. The scrubber operation guidelines are followed. After a certain number of operations, the liquid from the scrubber is collected in a large tank and then transferred as a chemical waste to the environmental affairs facility.

(ix) Gas Sensors

2 types of gas sensors are used in the lab. One is installed as the part of the facility in the lab which monitored the level of hydrogen sulfide all the time. This is connected to the central alarm system for protection in case of any accident in the level. This sensor is a bit away from the furnace and situated near the ground.

The other sensor is a hand held sensor which is turned on only before flowing hydrogen sulfide into the furnace until the end of the experiment. This sensor is always kept very close to the furnace or other places where the probability of leaking is high. Both the sensors triggered alarms at 3, 5 and 10 ppm of H_2S. But as H_2S has a very distinct smell, it is easier to detect the presence of H_2S immediately in case of any leaking even before the sensor is triggered.

(x) Sinton Lifetime Tester

Minority carrier lifetime (τ) is an important parameter in the determination of performance of solar cells as mentioned in chapter 2. In the lab, Sinton lifetime tester is used which follows Quasi-Steady-State Photoconductance (QSSPC) method. The tester came with a number of reference cells which could also be used for the calibration of the tool. The operation of this tool is performed according to the manual provided.

Along with the components mentioned above there are some other equipment like set of beakers, stirrer, hot bath, electronic weighing machine, thermometer, specific tweezers for each step of operation etc.

3.4 Recipe of Hydrogen Sulfide Passivation

The experimental set up for bulk passivation consisted of 3 main steps: cleaning of wafers, diffusion of H_2S gas and surface passivation by Al_2O_3. For another part of the experiment, annealing is also performed later after lifetime measurement on sulfur or hydrogen passivated samples. In this section, the passivation recipe steps have been mentioned step by step.

(i) Preparation and Cleaning of the Samples

The starting material or the samples came from multicrystalline silicon wafers 'As-Cut by wire saw' which were 125 mm × 125 mm in size. The wafers had the thickness of 300 μm for each as were Boron doped. The resistivity varied from 0.5 to 20 Ωcm. The wafers are cut into small sizes of 2-2.5" in length and less than 1.5" in width. During cutting the wafers in smaller pieces, care is taken so that no extra contamination is caused by any metal contact with the wafers.

For the preparation of the samples, a proper cleaning is a must to have any meaningful results which can be explained. Without cleaning steps, the target particles cannot be diffused into the grain boundaries of the samples. To ensure the reliability of the experiments, all the samples had to undergo 3 steps of ex-situ surface cleaning which has been described here:

A. Removal of Damaged Layer by Wire Saw:

As all the ordered wafers are as-cut, there would be damage layer of ~6 µm due to the wire saw cutting which had to be removed. For this 30% sodium hydroxide (NaOH) solution is used. In a 1 L beaker, almost 300 to 400 mL 30% solution is prepared and then heated using the hot plate up to 80 °C under the safe hood. The magnetic stirrer is rotated at a rate of 100 to 150 per min to maintain the uniformity of the solution.

The samples are first rinsed in clean deionized (DI) water to remove any dust or particle on the wafers. After the temperature reached 80 °C, the samples are soaked into the solution for 5 min. The etching rate is almost 1 µm/min. After that the samples are rinsed in the DI water to remove any remaining alkali solution.

B. Metal Removal

Normally in a mc-Si sample, metal contamination is common. Due to the use of wire saw or the damage removal step (where metal hydroxide is used), this metal removal step is a part and parcel for cleaning. For this stage, RCA-2 cleaning procedure is followed. RCA-2 solution is the mixture of 1 part 27 % hydrogen chloride (HCl), 6 parts water (H_2O) and 1 part 30 % hydrogen peroxide (H_2O_2).

300 ml of DI water is put in a Pyrex beaker and 27% 50 ml HCl is added very carefully to the solution. The solution is heated up to 70 °C using hot bath and magnetic stirrer is used like in the previous step. After the temperature reached 70 °C, 50 ml H_2O_2 (30%) is added with it. After the bubbles in the solution, the samples that already went through the stage of damage removal are soaked into it for 10-15 minutes. When the cleaning is finished, the samples are removed and rinsed with clean DI water. Then the samples are dried using the nitrogen to

remove any remaining solution or water and then preserved in the clean wafer-holders where they are kept till the final stage of cleaning.

C. Native Oxide Removal

Both c-Si and mc-Si samples grow a native silicon dioxide (SiO_2) very quickly on them even if they are kept for a very short time in the open air. So this step of cleaning is done when everything else in the lab is ready for the diffusion experiment and all the previous cleaning steps are finished on the samples. For this stage, 2% hydrogen fluoride (HF) solution is prepared in a Teflon tank. The samples are soaked into the solution for 1-2 min and then dried with nitrogen properly under the hood to keep away from air or any moisture content.

The following table 3.1 summarizes the cleaning steps mentioned here.

Table 3.1: Cleaning Steps of Multicrystalline Silicon Samples

Step No	**Step Name**	**Solution**	**Temperature (°C)**	**Time (minutes)**
1	Damage layer removal	NaOH (30%)	80	5
2	Metal removal-RCA2	$HCl/H_2O_2/H_2O$ (1:1:6)	70 – 80	10 – 15
3	Native oxide removal	Dilute HF HF/H_2O (1:50)	25	1 – 2

(ii) Diffusion of Hydrogen Sulfide in Grain Boundaries of the Samples

Before starting the experiment, it is made sure that the isolation and metering valve both are closed and also the valve in the vacuum pump is closed. A flowchart of the procedure has been mentioned in figure 3.1 which gives the whole scenario.

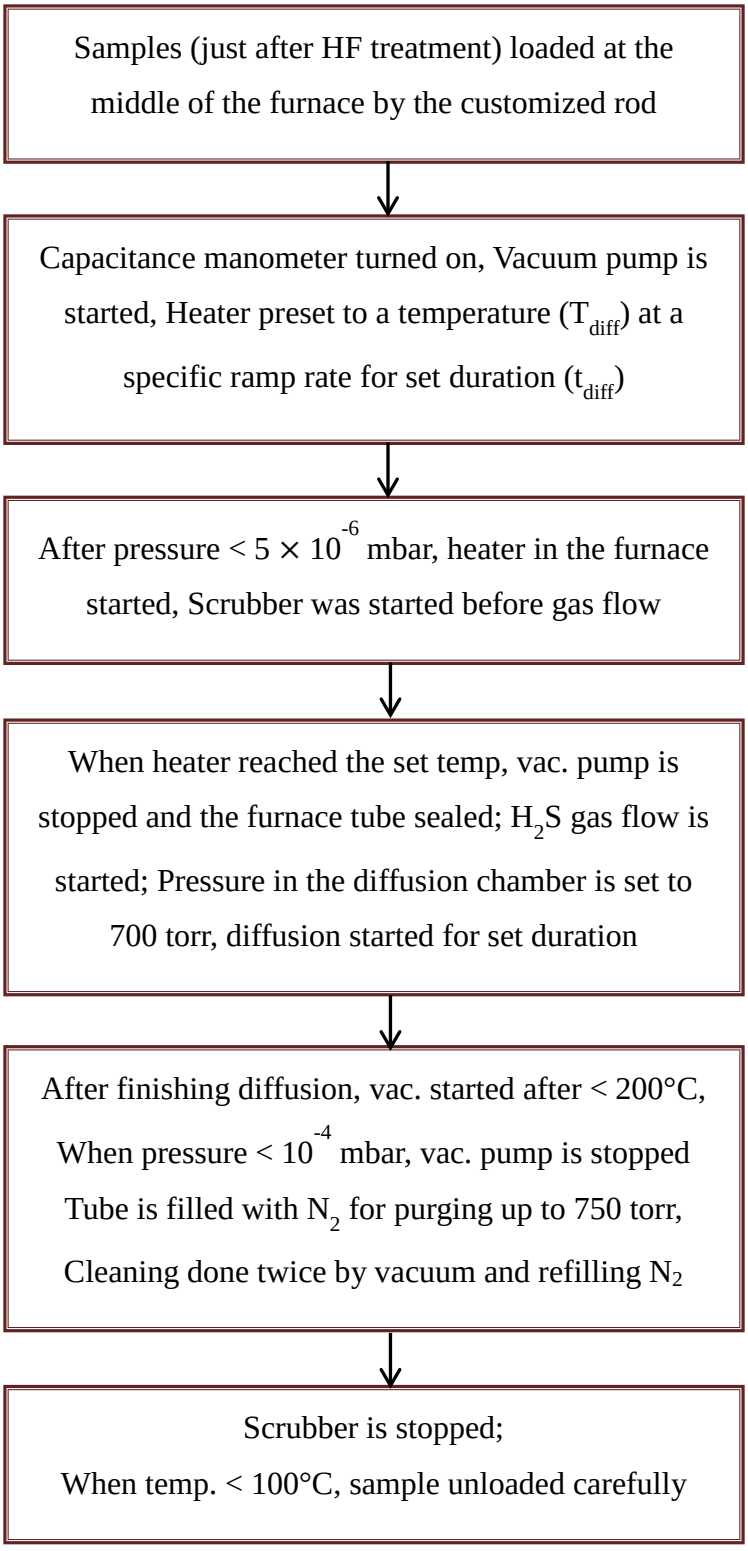

Figure 3.1 Flowchart Showing Diffusion of H_2S in mc-Si Grain Boundaries

In the procedure, the parameters t_{diff} and T_{diff} are changed to find out the best condition for passivation.

(iii) Surface Passivation with Aluminum Oxide by Atomic Layer Deposition

After the diffusion of H_2S in mc-Si samples, they are kept in small wafer holders till the next step of Aluminum Oxide (Al_2O_3) passivation. Before surface passivation, another round of 2% HF treatment for 1-2 min is performed to remove native oxide from the samples. A 10-nm Al_2O_3 film is deposited on both sides of the polycrystalline silicon by atomic layer deposition (ALD) at a substrate temperature of 200°C. Trimethyl Aluminum, also called TMA [$Al(CH_3)_3$] and water (H_2O) are the precursors for Al_2O_3 deposition through the following chemical reactions:

Reaction 1: Surface-OH + $Al(CH_3)_3 \rightarrow$ Surface-O-$Al(CH_3)_2$ + CH_4

Reaction 2: Surface-O-$Al(CH_3)_2$ + $2H_2O \rightarrow$ Surface-O-Al-$(OH)_2$ + $2CH_4$

Pulse durations are 0.015 seconds for TMA and 0.015 seconds for H_2O. The flow rate of N_2 carrier gas is 20 sccm, and the chamber base pressure is around 150 mtorr. The Al_2O_3 thin film is utilized to passivate the surface of mc-Si samples.

(iv) Lifetime Measurement

The initial conditions are set in the lifetime tester and the ready samples are measured following the operation manual. Lifetime is measured for both sides of the samples and then the average is noted down for the further analysis.

(v) Post-Annealing

After the measurement of lifetime, the samples that gave the highest lifetime are used for another round of post annealing in the furnace. The annealing is performed in open air. The post annealing temperature varied from 250 °C to 650 °C with

50 °C interval. Now after every annealing, the lifetime is measured and noted down and the samples are again loaded back for the annealing. Thus the effect of post annealing on the bulk passivated samples could be analyzed.

3.5 Recipe of Bulk Passivation Using Hydrogen by FGA Annealing

There are 2 reasons behind the experiment for bulk passivation by hydrogen. The first one is the comparison of quality of passivation between hydrogen sulfide and hydrogen. Another reason is the fact of finding out proofs of hydrogen's influence in H_2S passivation because both sulfur and hydrogen could contribute towards the bulk passivation. This has been covered in details in chapter 4 in the analysis section.

Now the procedures for hydrogen passivation starts with the same cleaning procedures followed in H_2S passivation mentioned here in 3.3. And after the passivation the samples go under the same Al_2O_3 passivation and lifetime measurement and post annealing steps. So only the diffusion recipe has been mentioned in this part.

For hydrogen passivation, the popular forming gas annealing (FGA) method was used in the lab which has already been detailed in 2.3. For conducting the FGA annealing, the chamber of an existing CVD system is used which has the facility for flowing the required gas over the samples in a very clean environment with good control over time, temperature and pressure.

After cleaning the samples, they are loaded in the chamber and vacuum pump is started. The heater is started to the diffusion temperature. At the same level of pressure mentioned in the previous section and at the set temperature, vacuum pump is stopped. 5% forming gas is then flown into the chamber for a set duration of time. After the FGA process, the chamber is purged with nitrogen before unloading the samples. Then the

samples undergo the same procedures like mentioned before. After measurement of lifetime and post annealing of the samples, the steps are complete and the collected data is ready for analysis.

3.6 Summary

The bulk passivation recipe using hydrogen sulfide has been described in details. Along with that the procedures followed for hydrogen passivation for mc-Si samples has been mentioned which is done for the sake of analysis and comparison. Quality of passivation obviously depends largely upon the procedures followed. So the results and analysis section are totally dependent on the design of the experiments.

CHAPTER 4

RESULTS AND ANALYSIS

4.1 Introduction

In this chapter, the data from the measurements have been analyzed. First the method of lifetime gain calculation has been described which is followed for all the analysis. Experiments on bulk passivation seemed to improve lifetime which gives an idea about the quality of the passivation. Also a comparative analysis with hydrogen depicts a clear picture. The post-annealing experiments also provide significant results. Also the stability of both kinds of passivation and impact of post-annealing on stability is important. These topics have been presented in this chapter sequentially.

4.2 Calculation of Lifetime Gain

In this part the calculation of minority carrier lifetime gain with the lifetime tester has been presented for the clarification of understanding the results presented in the later sections. The sample after Al_2O_3 passivation or post-annealing is ready for lifetime measurement. The lifetime tester is started 30 min before the measurement. Once it is ready, the software is turned on and the instrument is ‘zeroed’ (which records the conditions without any wafer). The wafer thickness, resistivity, minority carrier concentration at which the lifetime to be recorded are given to the system as inputs.

After that the samples are mounted on top of the base of the lifetime tester. And light is flashed. After it records the values, sometimes adjustment of the graph is needed so light is needed to be flashed again. When the graphs are finally ready, the lifetime is noted down for further analysis.

For the experiment, the thickness of the wafers is 300 µm. The minority carrier concentration selected for measurement of lifetime is 5×10^{14} cm^{-3} which is used for all the measurements. Optical constant is selected to be 0.7 which is normally used for both p-type and n-type wafers. After the measurement information like lifetime, sheet resistance etc. are calculated by the tool and printed on the screen. In figure 4.1, one of the graphs from an experimental result has been presented here.

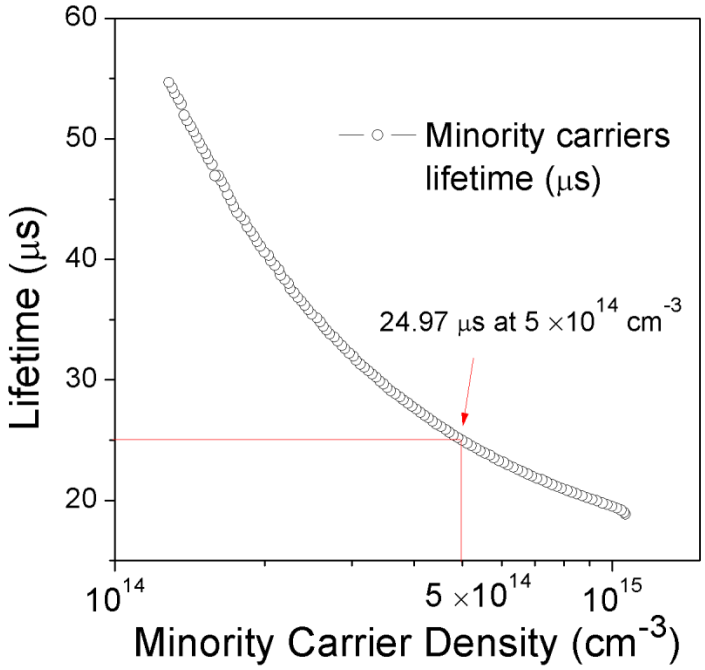

Figure 4.1 Minority Carrier Lifetime vs. Minority Carrier Density for Passivated Sample

The lifetime is then normalized by the base value of the control sample. For example, the lifetime from the above graph for the sample is 24.97 µs. The control sample from the same wafer showed a lifetime of 0.37 µs. So the lifetime gain for the current sample is (24.97/0.37) × 100% or ~6750%.

4.3 Analysis of Lifetime after H_2S Diffusion Experiment

(i) First Phase:

The first set of experiment of hydrogen sulfide diffusion was done with no previous idea about the exact experimental conditions. In this stage, the diffusion temperature (T_{diff}) was varied from 400 to 600 °C with a 50 °C interval. Two sets of experiment were performed where 2 diffusion times (t_{diff}) were used- 20 minutes for the first set and 40 minutes for the second set. So in total 10 samples were needed which came from a single mc-Si wafer just to make sure that all the samples had the same resistivity and same initial lifetime and so the results are directly comparable. And all of them went under same cleaning steps, HF treatment and Al_2O_3 surface passivation.

To compare the lifetime from H_2S passivated samples, a control sample from the same wafer is also prepared. This control sample also went under the cleaning steps and Al_2O_3 surface passivation, just the passivation step was skipped. Now the lifetime of the control sample is used as the base which indicates the lifetime of just surface passivated sample and all the lifetimes from both grain boundary and surface passivated samples are normalized on the control sample basis which gives the order of improvement through 'only' bulk passivation.

From the figure 4.2 significant improvement of lifetime of at least one order is distinguishable which also indicates the quality of the bulk passivation achieved by H_2S. For 20 min highest lifetime gain is ~1017 % and for 40 min highest lifetime gain achieved is ~934 %. Also in the graph, two distinct peaks can be seen in the lifetime gain vs temperature graph. One peak is at ~450 °C and the second peak at ~550 °C.

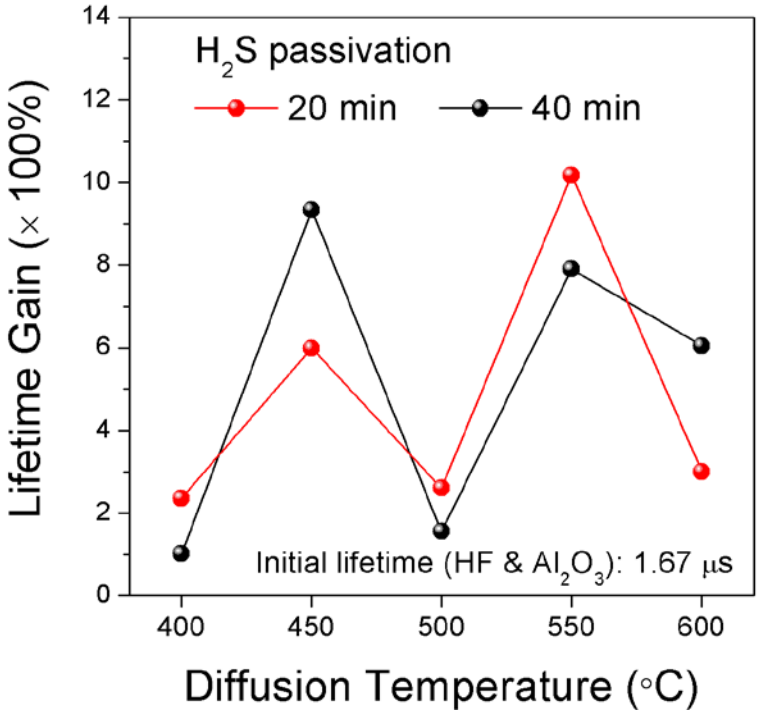

Figure 4.2 Lifetime Gain as a Function of Diffusion Temperature for H_2S

(ii) Second Phase

Now the result of the first phase of experiments directed to go through the second set of experiments to confirm the unique phenomenon of 2 peaks at two temperatures. So the experiment was repeated with another mc-Si wafer. A smaller temperature interval of 25 °C is chosen this time and the temperature range is unchanged. The diffusion is done for 40 min. So 9 samples were needed for this and like before they all were from the same wafer. Also for these samples, the collected data of lifetime are normalized on the basis of the lifetime of the control sample. In the next page the analysis for the second phase has been presented.

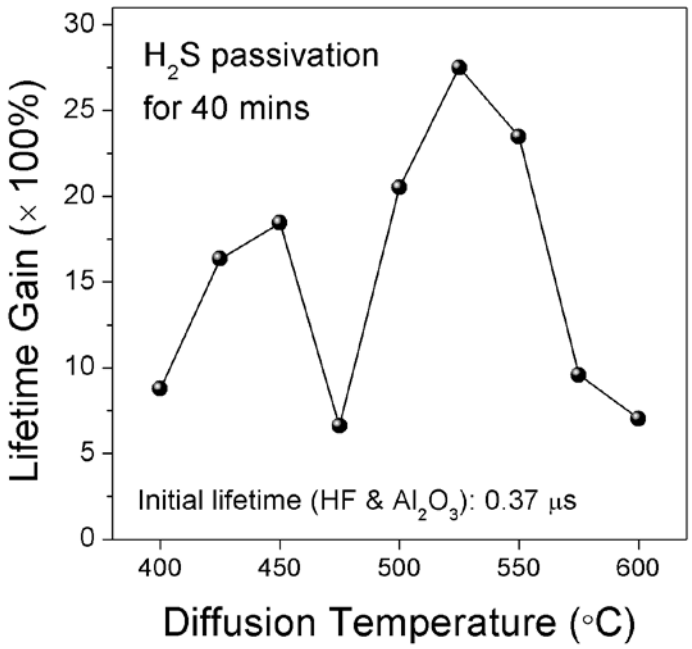

Figure 4.3 Lifetime Gain vs. Temperature for H_2S with Smaller Temperature Interval

From Fig 4.3, the lifetime measurement again shows two peaks roughly at the same regions ~450 °C and ~550 °C. The lifetime gain at ~525 °C is ~2750% and at ~550 °C is ~2347%. At the other peak of ~450 °C the gain is ~1844 %. The minimum lifetime gain at ~475 °C is ~660 %. The results suggest that a significant portion of the dangling bonds at the grain boundaries have been terminated and proves the effectiveness of H_2S in grain boundary passivation for mc-Si samples. These results raised two questions:

1. Why there are 2 peaks in the lifetime gain graph?
2. Is the effect of passivation happening due to the presence of hydrogen or sulfur in H_2S?

To answer these questions, the next set of experiment was developed. Grain boundary passivation was done by forming gas annealing (FGA) to study the effect of only hydrogen in the grain boundaries and eliminate any effect from sulfur.

4.4 Analysis of Lifetime after Hydrogen Passivation

During the design of this experiment, it is always kept in mind that the results of the hydrogen passivation could only be compared if the experimental conditions are kept same. From the literature review of hydrogen passivation [24, 29], it seems that FGA is mainly done in the range of 400 to 450°C. For the sake of comparison, here the chosen range for FGA annealing was from 300 to 600 °C. The diffusion time is 40 min to compare the results from H_2S passivation. Like H_2S passivation, all of the samples went under same cleaning steps, HF treatment and Al_2O_3 surface passivation.

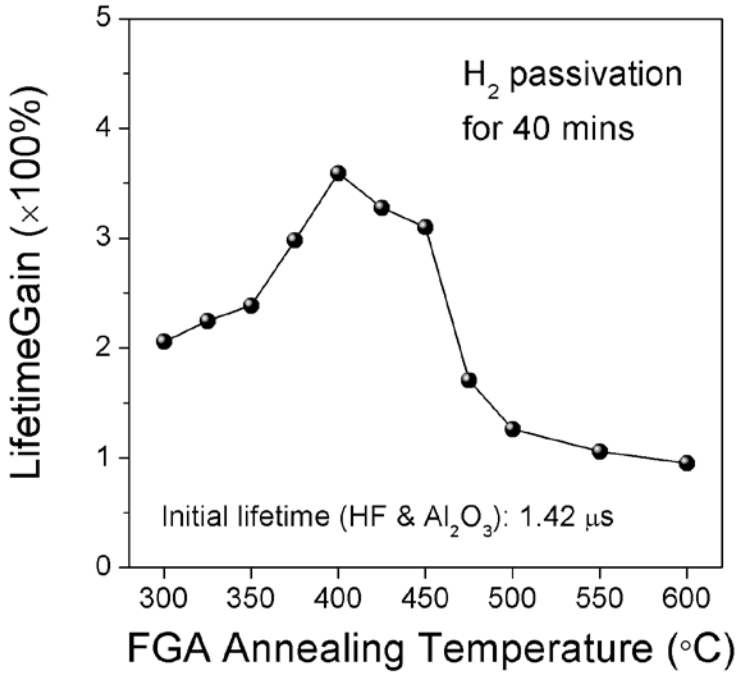

Figure 4.4 Lifetime Gain vs. Temperature for Passivation by H_2

From the Figure 4.4, hydrogen passivation also shows improvement of lifetime compared to the control sample of the same wafer. But the quality of passivation is inferior to H_2S indicated by the lower gain. The peak gain achieved at ~400 °C is ~359% which is lower compared to the gain from H_2S passivation (~2750% from one and

~934% from another experiment). Another observation from the graph is that it has only one peak that appeared ~425 °C. So from the results, it can be concluded that the second peak in the Fig 4.2 and 4.3 happens due to passivation effect from sulfur and the first peak happens due to the H_2 passivation. Also sulfur is more effective in passivation.

4.5 Analysis of Effects after Post-Annealing

(i) Post-Annealing of Passivated Samples

Post-annealing in ambient is another effective way to improve lifetime further [24,27,29]. To study the effect of post-annealing, both H_2S passivated and H_2 passivated samples are used for post annealing in the air. For both cases, the samples that provide the highest lifetime during passivation are used for post-annealing. The temperature was varied from 250 to 650 °C at a 50 °C interval.

Figure 4.5 shows the lifetime gain vs. post-annealing temperature graph for H_2S passivation performed at 450, 525 and 550 °C. 425 °C sample came from the first experiment (result shown in Fig 4.2) which shows the highest lifetime gain and also represent the peak due to hydrogen in H_2S. 525 and 550 °C samples came from the second experiment (result shown in Fig 4.3) which show the highest lifetime gain and also represented peaks due to sulfur, not Hydrogen.

From the figure 4.5, it is obvious that the lifetime gain increases first and then decreases for all the samples. The sulfur passivated samples show very high lifetime gain after post-annealing and the best gain is ~6750 % at 500 °C which is ~2.5 fold improvement compared to passivated samples (from fig 4.2 lifetime gain ~2750%). Even for the peak due to hydrogen showed high lifetime gain of ~2500% which is ~2.5 fold improvement (from Fig 4.1, lifetime gain ~934%) after post-annealing.

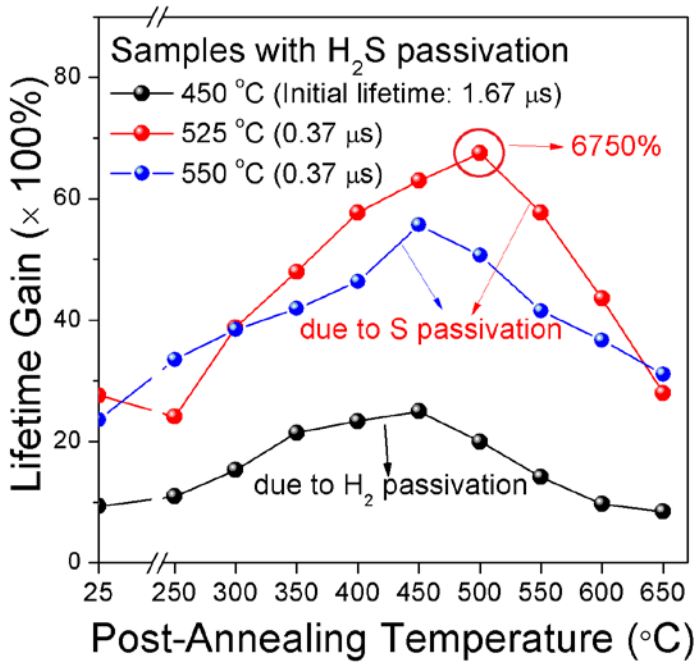

Figure 4.5 Lifetime Gain vs. Post-Annealing Temperature after H_2S Passivation

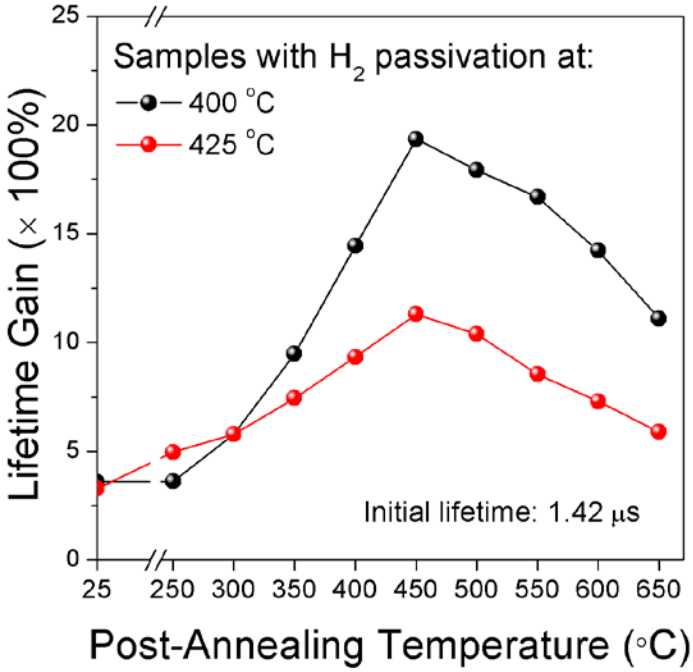

Figure 4.6 Lifetime Gain vs. Post-Annealing Temperature after H_2 Passivation

Figure 4.6 shows the lifetime gain vs. post-annealing temperature graph for H_2 passivation performed at 400 and 425 °C which show the highest lifetime gain (result

shown in Fig 4.4). The trend of lifetime gain graph is same as post-annealing after H_2S passivation in figure 4.5. After post-annealing, the best gain is for the 400 °C passivated sample and the gain is ~1935 % at 500 °C which is almost 5 fold improvement over passivated sample (from fig 4.4 lifetime gain ~359%).

(ii) Post-Annealing of Control Samples

For the comparison, post-annealing is performed also on control samples which are used earlier as the basis for calculation of lifetime gain. As mentioned before, these control samples underwent all cleaning steps and Al_2O_3 surface passivation. From figure 4.7, a lifetime gain of ~754% at 450 °C is seen. The trend of the graphs in 4.5, 4.6 and 4.7 is also quite similar. So lifetime gain after post-annealing cannot be attributed to either sulfur or hydrogen, rather its contribution depends on the quality of Al_2O_3 passivation.

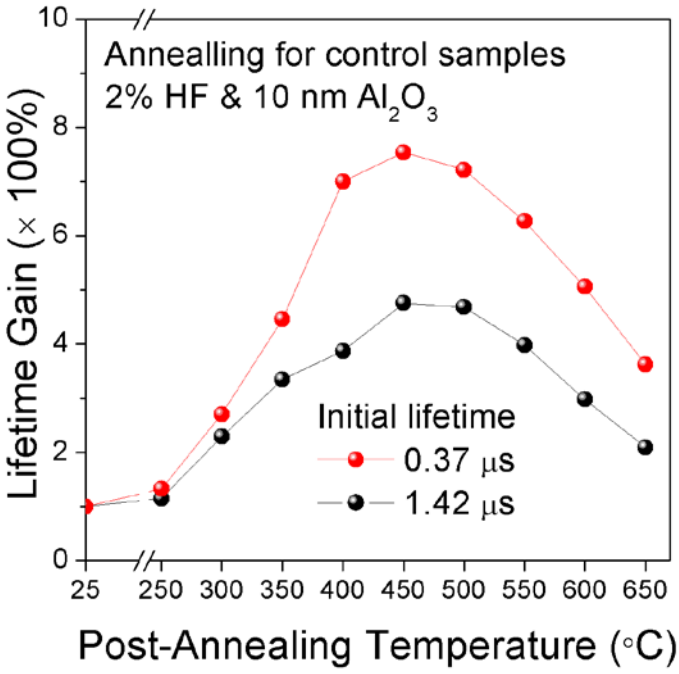

Figure 4.7 Lifetime Gain as a Function of Post Annealing Temperature for Control Samples without H_2S or H_2 Passivation

The lifetime improvement for Al_2O_3 surface passivated samples after post-annealing was also reported by [45,46] for c-Si samples. The results of their experiment match with the above mentioned experiment which means that the quality of surface passivation probably increases due to post-annealing as it takes care of a lot of damages in the bulk created during the experiments [27,34,35].

So from the above analysis, it can be said that grain boundary passivation by sulfur is more dominating than hydrogen. Sulfur passivation at ~550 °C contributes to higher gain. Post-annealing further improves lifetime gain but at this stage Al_2O_3 is mainly responsible for the improvement.

4.6 Stability of Lifetime

To compete with the current bulk passivation schemes, a newly proposed passivation scheme needs to be stable with the passage of time. That is why in this section, the stability of lifetime for samples of different condition has been studied.

For this study, samples which were characterized just after Al_2O_3 surface passivation or post-annealing are kept in the lab. After ~2 months their lifetimes are measured again to check for any changes. In Table 4.1, the results of lifetime gain for samples that underwent different experimental conditions have been presented for understanding.

Table 4.1: Lifetime Gain for Different Samples: As-Passivated and after ~60 Days

	Number of Samples	**Lifetime gain (× 100%) As-passivated**	**Lifetime gain (× 100%) After ~60 days**	**Average decrease (in %)**
H_2S passivated	3	20.5	15.45	26.37
		23.23	16.9	
		16.35	11.9	
H_2 passivated	3	2.97	2.35	22.45
		3.09	2.29	
		2.38	1.89	
H_2S passivated and post-annealed	3	31.11	29.61	5.067
		28	25.59	
		8.46	8.31	
H_2 passivated and post-annealed	2	11.09	10.42	5.483
		5.89	5.6	
Control sample post-annealed	2	3.62	3.48	4.805
		2.09	1.97	

Now from the table, it is observed that bulk passivated samples without post-annealing have lost almost ~25% of the earlier recorded lifetime. This happens due to the instability of bulk passivation as also observed by Muller et al [27]. But even after this instability H_2S passivated still show significant gain of as high as ~1500 % compared to the gain of ~230% from H_2 passivated samples.

When it comes to the post-annealed samples, all of the samples show better stability. For H_2S passivated or H_2 passivated samples, the lifetime decreased only by ~5% or less. To find out the reason, the control samples which underwent post-annealing

are measured. As can be seen from the table, the control samples (with Al_2O_3 passivation) with ‘no’ bulk passivation also show good stability with time. So it can be said that post-annealing contributes to higher lifetime gain and also the stability of passivated samples and thus would be a very important step if this process is in use.

The reason behind the instability of sulfur and hydrogen in grain boundaries is the desorption of atoms from the grain boundaries. The desorption of sulfur atoms is slower than hydrogen normally but over time, both of them come out of the grain boundaries and the device tend to retain its initial characteristics. Now when post-annealing is performed, there is a major change in the bulk. Some of the atoms come out of the grain boundaries and others are placed randomly in empty sites. After the process, the grain boundaries are more stable, because evidently sulfur or hydrogen atoms sit at more convenient gaps than usual which makes the desorption slower as it requires more energy to come out of those lower energy states. Thus the passivation quality increases for post-annealed samples and the system is more stable.

4.6 Conclusion

This chapter summarizes all the experimental results from the experiments performed in chapter 3. The results indicate the quality of passivation through improvement of lifetime, further improvement through post-annealing attributed to Al_2O_3 passivation and also stability improved by post-annealing of the passivated and unpassivated samples.

CHAPTER 5

CONCLUSIVE REMARKS

In this chapter a summary of the total project has been presented. Along with some remarkable achievements in the project, future scopes of research work in this line of work has been mentioned. In spite of the challenges faced due to the novel nature of the experiment, the design of the experiment was good enough to achieve the results.

5.1 Summary of the Work

- Benefits of sulfur as element and a good compatible surface passivation (Al_2O_3) led to the design the experiment for grain boundary passivation of multicrystalline silicon (mc-Si) using H_2S.
- Decent quality of passivation is achieved through grain boundary passivation of H_2S in mc-Si samples yielding high minority carrier lifetime gain (~2750%) around ~550 °C
- In the minority carrier lifetime gain vs. temperature graph for H_2S passivation, two peaks are observed- one peak at ~450 °C and the second one at ~550 °C
- Bulk passivation by H_2 shows one peak at ~450 °C and lifetime gain is much lower (~359%) compared to H_2S.
- Sulfur in H_2S may be dominant for improvement in lifetime and also responsible for the second peak whereas hydrogen is supposed to be responsible for the first peak consolidated by the proof from the trend of the post-annealing data.
- Post-annealing improves the lifetime gain for all passivated samples. The highest lifetime gain achieved is as high as ~6750 % which is achieved at post-annealing temperature of ~500 °C.

- Same trend is observed for all samples for the post-annealing lifetime gain vs temperature graph. This led to the experiment of post-annealing of control samples and similar trend is observed in control samples.
- Before annealing, sulfur passivation is dominant but for post-annealing improvement, Al_2O_3 surface passivation is responsible for further improvement.
- Stability of lifetime gain for only passivated samples is not very high. After ~60 days of experiment it decreased by ~25% of the previously recorded lifetime for both H_2S and H_2 passivated samples.
- Post-annealing improves lifetime for all passivated and control samples because post-annealing of Al_2O_3 passivated samples evidently contributes to stability.

5.2 Discussion

A novel approach for grain boundary passivation in multicrystalline silicon (mc-Si) by using hydrogen sulfide has been proposed in this research work. Benefits of sulfur as element and its earlier success for surface passivation in crystalline silicon (c-Si) motivated us in this research. A completely new set of experiment has been designed for passivation of mc-Si samples. Experiments were carried out under varied conditions with the objective to find out the best combination to achieve the highest lifetime. The attempts are successful since the minority carrier lifetime gain achieved through H_2S passivation is higher compared to H_2 passivation. A compatible surface passivation by Aluminum oxide (Al_2O_3) is also proposed in this work. The combined effect of Al_2O_3 with grain boundary passivation not only increases lifetime gain but also contributes to higher gain after post-annealing and makes the samples stable, thus the total procedure becomes more reliable. As lifetime is related to internal quantum efficiency (IQE) of

solar cells, higher IQE is anticipated if the proposed technique is incorporated in mc-Si solar cells. In addition to this, the diffusion procedure of H_2S in the lab is a cost effective process since it does not require any expensive equipment. Moreover, taking care of the chemical waste from the experiment is inexpensive and straightforward. Therefore it can be concluded that the proposed techniques of grain boundary passivation could be a feasible solution although additional research is required before it can have commercial implementation in solar cells.

5.3 Future Scope of Work

As demonstrated in the experiments, grain boundary passivation by H_2S seems to have potential for success as a technique of passivation. The real challenge for now is to incorporate this technique and make solar cells out from the bulk and surface passivated wafers. For that the diffusion experiment would need some modification as the experiments done here were performed on smaller samples. Also when bigger samples would be used, uniformity of diffusion temperature would be tougher to achieve. So keeping all these in mind, it can be said that there are lots of room for work in this field if this bulk passivation technique has to be used for mc-Si solar cells.

REFERENCES

[1] International Energy Agency, World Energy Outlook (2012).

[2] International Energy Agency, Key World Energy Statistics (2013).

[3] Hoffert et al, M.I. Hoffert, K. Caldeir, A.K. Jain, E.F. Haites, L.D.D. Harveyk, S. D. Potter, M.E. Schlesinger, S.H. Schneider, R.G. WattsI, T.M. L. Wigley and D.J. Wuebbles, Nature, **395**, 881 (1998).

[4] N. S. Lewis, and D.J. Nocera,, Proc. Natl. Acad. Sci. **103**, 15729 (2006).

[5] U.S Dept. of Energy, Basic Research Needs for Solar Energy Utilization (2005).

[6]A.E.Becquerel, Mémoire sur les effets électriques produits sous l'influence des rayonsolaires. Comptes Rendus des Séances Hebdomadaires,. **9**, 561 (1839)

[7] C.E. Fritts, on a New Form of Selenium Photocell, Proc. of American Assoc. for the Advancement of Science. (1883)

[8] R.Ohl, U.S. Patent No 2,402,662, Washing, DC. “Light Sensitive Device”.

[9] D.M. Chapin, C.S. Fuller, and G.L. Pearson, J. Appl. Phys. **25**, 676-677 (1954)

[10] A.W. Blakers, and M.A. Green, Annual Conf., ISES (ANZ Section) (1985)

[11] U.S. National Renewable Energy Laboratory, Record Cell Efficiency

[12] A.G. Aberle, Prog. Photovolt: Res. Appl. **8**, 473, (2000)

[13] PV Education.org, retrieved from http://pveducation.org/pvcdrom/

[14] C. H. Seager, and D. S. Ginley, Appl. Phys. Lett., **34**, 337 (1979)

[15] J.Y. Lee, S.W. Glunz, Sol. Energy Mater. & Sol. Cells, **90**, 82 (2005)

[16] A. K. Ghosh, C. Fishman, and T. Feng, J. Appl. Phys., **51**, 446 (1980)

[17] A.K. Ghosh, and T. Feng, J. Appl. Phys. **49**, 5982 (1978).

[18] J.Y.W. Seto, J. Appl. Phys. **46**, 5247 (1975).

[19] C.H. Seager, and T.G. Castner, J. Appl. Phys. **49**, 3879 (1978).

[20] C. Baccarani, B. Ricco, and G. Spadure, J. Appl. Phys. **49**, 5565 (1978).

[21] G. Dingemans, and W. M. M. Kessels, J. Vac. Sci. Technol. A, **30**, 040802 (2012);

[22] W.Shockley, *Electrons and Holes in Semiconductors*, Wiley, New York, p. 318-325 (1959).

[23] H.C. Card, and E. Yang, IEEE Trans. Electron Devices, **ED-24**, 397 (1977).

[24] J. C. Muller, Y. Ababou, A. Barhdadi, E. Courcelle, S. Unamuno, D. Salles, And P. Siffert, J. Fally, Sol. Cells, **17**, 201(1986)

[25] R. Lüdemann, Mater. Sci. Eng., B, **58**, 86–90 (1999)

[26] L. Ammor, and S. Martinuzzi, Solid State Elect., **29**, 1 (1986)

[27] J. C. Muller J.C. Muller, Vu Thuong Quat, P. Siffert, H. Amzil, A. Barhdadi, N. M'Gafad, Sol. Cells, **25**, 109 (1988)

[28] A. Barhdadi, H. Amzil, J. C. Muller, P. Siffert, Appl. Phys. A, **49**, 233 (1989)

[29] P. Sana, A. Rohatgi, J. P. Kalejs, and R. O. Bell, Appl. Phys. Lett., **64**, 97 (1994)

[30] A.Rohatgi, P. Sana, and J. Salami, Proc. of the 11th European Photovolt. Sol. Energy Conf., Montreux, Switzerland, p.159 (1992)

[31] A. G. Aberle, Sol. Energy Mater. & Sol. Cells, **65**, 239 (2001)

[32] J. F. Lelièvrea, E. Fourmonda, A. Kaminskia, O. Palaisb, D. Ballutaudc, M. Lemitia, Sol. Energy Mater. & Sol. Cells, **93**, 1281 (2009)

[33] H.F.W. Dekkers, S. De Wolf, G. Agostinelli, F. Duerinckx, G. Beaucarne, Sol. Energy Mater. & Sol. Cells, **90**, 3244 (2006)

[34] W. Soppe, H. Rieffe, and A.Weeber, Prog. Photovolt: Res. Appl., **13**, 551 (2005)

[35] F. Duerinckx, J. and Szlufcik, Sol. Energy Mater. & Sol. Cells, **72**, 231 (2002)

[36] D.S. Ruby, W.L. Wilbanks, C.B. Fledderman, J.I. Hanoka, 13th European Photovolt. Sol. Energy Conf., Nice,p. 1412 (1995)

[37] B. L. Sopori, X. Deng, J.P. Benner, A. Rohatgi, P. Sana, S.K. Estreicher, Y.K. Park, M.A. Robertson, Sol. Energy Mater. Sol. Cells **41**, 159 (1996).

[38] G. Song, M. Y. Ali, and Tao, M., IEEE Electron Device Lett., **58**, 71, (2007)

[39] M. Y. Ali, and M. Tao, Electrochem. Solid-State Lett., **10**, H317 (2007)

[40] M.Y. Ali,and M. Tao, J. Appl. Phys., **101**, 103708 (2009)

[41] H. Zhang, A. Saha, W.C. Sun, M. Tao, Appl. Phys. A, **116**, 2031 (2014)

[42] E. Kaxiras, Phys. Rev. B 43, 6824 (1991)

[43] F. Wald, *Poly-Micro-Crystalline and Amorphous Semiconductors*, Les Editions de Physique, Les Ulis, France, p. 33, (1981)

[44] B. Cordero, V. Gomez et al., Dalton Trans., 2832 (2008)

[45] J. Benick, A. Richter, M. Hermle, and S. W. Glunz, Physica Status Solidi (RRL) – Rapid Research Letters, **3**, 233, (2009)

[46] B. Hoex, S. B. S. Heil, E. Langereis, M.C.M. van de Sanden, W.M.M. Kessels, Applied Physics Letters, **89**, 042112 (2006)